Supporting Information

Drescher et al. 10.1073/pnas.1000901107

SI Text

Culture Conditions. For all experiments, we used *Volvox carteri* f. *nagariensis* EVE strain, a subclone of the HK10 strain, kindly provided by A.M. Nedelcu (University of New Brunswick) and D.L. Kirk (Washington University, St. Louis). *V. carteri* were grown axenically in 50 ml of standard *Volvox* medium (SVM) (1, 2) in 125-mL Erlenmeyer flasks with sterile air bubbling. Experiments were performed with cultures that were grown up to a concentration of ~200 colonies per mL, after inoculating the culture with ~50 colonies. For the population assay, more organisms were required so that *V. carteri* were grown in 125 mL of SVM in 250-mL Erlenmeyer flasks. The culture flasks were kept in diurnal growth chambers (KBW400; Binder GmbH), where they were illuminated from above by cool white fluorescent light, in a daily cycle of 16 h of light at 28 °C and 8 h of darkness at 26 °C. The intensity of the growth light was ~4,000 lx, or 80 μmol of photosynthetically active radiation (PAR; light with wavelengths between 400 and 700 nm) photons $m^{-2}\,s^{-1}$ (see spectrum in Fig. S1).

Stimuli with an Optical Fiber. A schematic diagram of the sample chamber is given in Fig. S2*A*. The bottom and top surfaces are made from glass coverslips. The vertical spacer is a 3.2-mm outer diameter plastic tube glued to the glass by UV-curing optical glue (NOA68; Norland Products). The geometry of the chamber allows easy access from two perpendicular directions, as in Fig. S2*B*. The temperature was monitored by a thermistor attached to the sample chamber and found to be 24.5 ± 0.5 °C. All measurements were done in SVM.

To keep a *Volvox* colony in the field of view of the microscope for extended periods, it was caught with a micropipette by aspiration. The micropipettes were pulled from glass capillaries, shaped, and fire polished (with equipment from Sutter Instrument) to have a rounded tip of outer diameter ~100 μm, as in Fig. S2*B*. The untreated end of the micropipette was then inserted into a holder (PicoNozzle; World Precision Instruments), connected to a gas-tight syringe with micrometer control (Manual Injector; Sutter). The micropipette/holder assembly was mounted on a custom-made rotation stage, attached to a motorized micromanipulator (PatchStar; Scientifica). To stimulate reliably only the anterior part of a *Volvox* colony, it was necessary to rotate the micropipette until the anterior-posterior axis of the colony was in the focal plane. After some practice it was possible to catch organisms with their posterior-anterior axis approximately perpendicular to the axis of the micropipette, allowing a reorientation of the colony by pipette rotation to an orientation as shown in Fig. S2*B*. The anterior-posterior axis was found to be in the focal plane when the germ cells were grouped on one side of the colony (so that in the focal plane, the area of a polygon that encloses the projections of the germ cells is minimal) and when at the same time the posterior pole (as identified by the position of the germ cells) is opposite to the anterior flow stagnation point (as identified by inspection of the self-generated flow). The flow was visualized with 1-μm carboxylate-modified polystyrene beads (F8819; Invitrogen), suspended in SVM at a concentration of $\sim 1.4 \times 10^8$ beads per mL. Movies of the flow in response to a stimulus time series were recorded at 100 fps with a high-speed camera (Phantom V5.1; Vision Research), connected directly to a Nikon TE2000-U inverted microscope with a Nikon 10× (N.A. 0.3) objective in bright-field illumination. To avoid photoresponses due to the halogen lamp bright-field illumination (3–7), two identical long pass interference filters (each with a 10-nm transition between transmissions of $T = 10^{-3}$ and $T = 0.8$, centered at 620 nm; Knight Optical) were placed in the microscope beam path.

All stimuli were applied with a cyan LED (Luxeon V; Philips Lumileds; see spectrum in Fig. S1), coupled into a 550-μm-diameter optical fiber (N.A. 0.22, FG550LEC; Thorlabs) via a fiber launch station (MBT611/M; Thorlabs) with a 10× (N.A. 0.25) Olympus objective. The fiber was fed through a micropipette holder (PicoNozzle; World Precision Instruments) that was attached to a micromanipulator identical to the one used to control the micropipette position. The amount of light leaving the free end of the fiber was measured with a photodiode (DET110; Thorlabs) and could be controlled manually with an iris in the fiber-coupling beam path and electronically by sending modulation voltages (0–5 V) to the LED driver (LEDD1; Thorlabs). The electronic control allowed time-dependent stimuli to be produced with a time resolution better than 1 ms. The modulation voltage time series that provided the stimulus time series were written in LabVIEW and contained a triggering signal for the high-speed camera.

Flow speeds were measured from the recorded movies by particle image velocimetry (PIV), with an open source software package for Matlab (8). The PIV data were interpolated so that flow speeds could be read out 25 μm above the colony surface—i.e., approximately 10 μm above the flagellar layer. To get a single time series that represents the photoresponse of the colony, we averaged the flow speed time series between the angles −30° and +30° as measured from the anterior pole.

Measuring the frequency response. We supplied a sinusoidal light stimulus to the organism anterior, with a minimum light intensity of 1 μmol PAR photons $m^{-2}\,s^{-1}$ and a maximum of 20 μmol PAR photons $m^{-2}\,s^{-1}$. These values were chosen to be consistent with the population assay described below. Because the output of the LED was not quite linear in the modulation voltage, we calibrated the modulation voltage time series in such a way that the light intensity time series was sinusoidal. As the very onset of light emission was difficult to calibrate reliably, we chose to have a nonzero minimum light intensity. For each stimulus, the organism was stimulated for 30 s (or two periods, whichever was longer) directly before the recording began. Yoshimura and Kamiya (9) assumed that, to simulate the organism rotation for a *Chlamydomonas* cell, the most realistic stimulus would be a "half-sine"—i.e., a stimulus proportional to $H(\sin \omega_s t) \sin \omega_s t$, where H, ω_s, and t are the Heaviside step function, stimulus angular frequency, and time, respectively. In addition to using a sinusoidal stimulus, as shown in Fig. 3 of the main text, we also measured the photoresponse to half-sine stimuli. The data for both stimuli are compared in Fig. S3. It is evident that at low ω_s the high Fourier frequency content of the half-sine leads to a higher response, in comparison to the purely sinusoidal stimulus, where only a single frequency is present. For each organism, the responses were normalized by the organism's maximum response. The normalized responses were averaged across 16 organisms for the sinusoidal stimulus and 25 organisms for the half-sine stimulus.

Measuring the photoresponse for different light intensities. We measured the photoresponse as a function of the stimulus light intensity, for a stimulus frequency of 0.25 Hz. Instead of a sinusoidal stimulus we used a top-hat function, because this allowed the minimum light intensity to be zero. The organism was dark-adapted between each stimulus (i.e., movie) for 2 min. At each light intensity, the organism was stimulated with 20 periods before the recording began, and the response was recorded for

4 periods. When the flagellar beating (i.e., the measured flow speed) decreased upon an increasing stimulus light, the photoresponse was termed "positive" because it turns the organism toward the light, as discussed in the main text. A photoresponse was termed "negative" when the flagella beating decreased upon a decrease in stimulus light, because this will turn the organism away from the light. Negative photoresponses could be modeled with a similar dynamical system as the positive photoresponses, including the Heaviside function, so that we expect our theory to also hold for negative phototaxis. The transition from positive to negative phototaxis occurred between 100–250 μmol PAR photons m^{-2} s^{-1}. Interestingly, when organisms were dark-adapted, they displayed positive photoresponses even for the highest light intensities in the first ∼30 s of the stimulus time series and then switched to negative phototaxis. The response amplitude was taken as the amplitude of the oscillatory signal. For each organism, the responses were normalized by the organism's maximum response. The normalized responses were averaged across 16 organisms. A graph of the photoresponse as a function of stimulus intensity is shown in Fig. S4.

Measuring the two time scales. For this measurement *V. carteri* colonies were dark-adapted for at least 2 min and then exposed to a sharp increase in stimulus light intensity. The response was characterized with two time scales: the response and adaptation time scales. The model response was fitted to the flow speed time series to obtain τ_r and τ_a. The time scales were measured for 20 organisms.

Measuring the flagellar response probability. For this measurement we observed the flagellar behavior directly rather than observing the flow generated by the flagella. This allowed a more precise localization of the light-responsive region on the *V. carteri* colony. To visualize flagella, the high-speed camera recorded images at 200 fps, in red bright-field illumination ($\lambda > 620$ nm, obtained with filters as described above) using a Nikon 40× (N.A. 0.6) air objective. The organism was held on a rotatable micropipette, in the same geometry as in Fig. S2*B*, except that now the posterior pole was nearest to the optical fiber. The stimuli were a large step up in light intensity (from 0 to 1500 μmol PAR photons m^{-2} s^{-1}) and a corresponding step down 6 s later. Such a strong stimulus assured that even the somatic cells on the far side of the colony, as viewed from the optical fiber (i.e., those near the anterior pole), received a strong enough stimulus to display a significant photoresponse. A whole *Volvox* colony has been measured to attenuate light of 490 nm by a factor of ∼2 (10), and an individual *Chlamydomonas* cell (which is similar to a *Volvox* somatic cell) has been measured to attenuate light of 495 nm by a factor of ∼8 (11, 12), yielding a minimum stimulus amplitude on the far side of the colony of ∼90 μmol PAR photons m^{-2} s^{-1}. A "response" was defined as a change in the flagellar beating period (periods were measured manually) following a step stimulus. Often the flagella slowed down so much that they stopped completely, as previously described by Gerisch (13) and Huth (10). Because the axis of the organism was in the focal plane, we could measure at which polar angles θ (where $\theta = 0$ is the anterior pole) a *V. carteri* colony is responsive to light. This measurement was performed on 35 young colonies, just after they hatched.

Measuring the Eyespot Size. A *V. carteri* colony was caught and held with a micropipette, using the same equipment and sample chamber as described above. To obtain high resolution images of the somatic cells and their eyespots, a Nikon 60× (N.A. 1.4) oil objective with differential interference contrast optics was used. Photographs were taken with a digital single-lens reflex camera (Nikon D300) directly connected to the microscope. The *V. carteri* colonies were caught with their posterior-anterior axis almost exactly perpendicular to the axis of the micropipette. By rotating the holding micropipette and focusing on the colony surface, it was thus possible to move the anterior pole into the focal plane (see Fig. S5*A*). By rotating further, while keeping the focus on the colony surface, the eyespot size could be measured as a function of the polar angle θ (see Fig. S5*B*). In the images of the eyespots, the largest diameter was taken to be the eyespot size. For $\theta \gtrsim 110°$, eyespots could not be clearly distinguished within the somatic cells, and eyespot sizes are thus not given for these angles. Measurements were performed on 10 young colonies, just after they hatched. The somatic cells are precisely arranged in each colony (14–16). For all colonies, the images showed that the center of a somatic cell and the center of the eyespot are at the same longitude (Fig. S5 *A* and *B*), and that within a somatic cell the eyespot is placed further away from the anterior pole than the center of the somatic cell.

To gain further information on the eyespot placement in the somatic cells, we observed the somatic cells on the *Volvox* perimeter while the posterior-anterior axis was in the focal plane (the organism orientation was as in Fig. S2*B*). This yielded photographs similar to the schematic diagram in Fig. S5*C*. These photographs allowed us to measure the angle κ (defined in Fig. S5*C*). For these measurements we ignored a possible dependence of κ on θ.

Measuring the Rotation Rate Dependence of the Phototactic Ability. For measurement of the phototactic ability as a function of the rotation frequency of *V. carteri*, we devised a population assay as follows. To control the rotation frequency we prepared solutions of SVM with various concentrations of methylcellulose (M0512; Sigma-Aldrich), the highest concentration being 0.65% (weight/weight). The macroscopic rheology of methylcellulose has been determined to be Newtonian at concentrations <1% (17). Rectangular Petri dishes (11.7 × 7.5 cm, Nunc 242811; Thermo Fisher Scientific) were then filled with 30 mL of SVM containing different concentrations of methylcellulose (yielding a bath of depth ∼3.5 mm).

At the beginning of a series of measurements to assess the phototactic ability at the various viscosities, a whole *V. carteri* culture that just hatched was removed from its Erlenmeyer flask in the growth chamber and placed into a custom-made large rectangular dish with a light on one side (the same type of LED we used for the stimuli delivered with an optical fiber). This light was used to select phototactic organisms (almost all colonies displayed strong phototaxis at this stage), which were placed into the rectangular Petri dish of a particular viscosity (and mixed on an orbital shaker for 4 min) just before the measurement. In this way, the phototactic ability was measured for organisms from the same culture, at different viscosities (and thus rotation rates). Pipetting was done slowly to avoid high shear rates which could rip flagella off the *V. carteri* surface.

To measure the phototactic ability, individual *V. carteri* colonies were tracked while the stimulus light was on. The schematic diagram in Fig. S6*A* illustrates the geometry of the experimental setup. A CCD camera (Pike F145B; Allied Vision Technologies) attached to a long working distance microscope (InfiniVar CFM-2/S; Infinity Photo-Optical) recorded movies at various frame rates (triggering was done through a pulse train generated with LabVIEW). The bright-field background illumination for the microscope was provided by a red LED (maximum at 655 nm, FWHM 21 nm, LFR-100-R; CCS Inc.). The light intensity that the stimulus light source provided in the field of view of the camera was measured to be ∼15 μmol PAR photons m^{-2} s^{-1}, yielding positive phototaxis. During the assay, temperature was measured with a thermistor attached to the rectangular Petri dishes and found to be in the range 24 ± 1 °C.

To obtain the phototactic ability, we computed the cosine of the angle of the swimming track with the light direction of each organism at every time step. The distribution of swimming angles with the light direction is given for two very different viscosities in

Fig. S6 *B* and *C*. Rotation rates were measured manually with the aid of a commercial image processing software (MetaMorph; Molecular Devices) by counting frames. For each viscosity and population, we measured ω_r for 20 colonies.

Details of the Mathematical Model. The mathematical model for phototaxis of *Volvox* relies only on measured parameters and is able to give detailed predictions of the swimming characteristics and the ability to turn toward the light. It is based on a knowledge of the fluid velocity at the edge of the flagellar layer of *Volvox* and how this fluid velocity changes when parts of the surface are exposed to a light stimulus.

The coupled equations that make up the model are given in the main text. To determine the time evolution of the system of coupled equations, we solved the coupled partial differential equations for $p(\theta,\phi,t)$ and $h(\theta,\phi,t)$ numerically with a built-in solver in Mathematica (Wolfram Research) between times t and $t+\delta t$. Due to the integral in the equation for $\mathbf{\Omega}$, we used an Euler method to then solve the equation for $\hat{\mathbf{I}}(t)$ at every time step. We ensured convergence of the results by choosing a small enough step size δt.

In addition to finding the angle of the *Volvox* axis with the light direction, the model can also be used to determine the organism swimming velocity $\mathbf{U}$, via another result from Stone and Samuel (18)

$$\mathbf{U}(t) = \frac{1}{4\pi R^2}\int \mathbf{u}(\theta,\phi,t)dS, \qquad [S1]$$

which allows trajectories of the organism to be reconstructed.

A solution of the photoresponse $p(\theta,\phi,t)$ is plotted in Fig. 6 of the main text, using the "reduced model" defined in the main text. A decomposition of this photoresponse into spherical harmonics $Y_l^m(\theta,\phi)$ is given in Fig. S7. The photoresponse p computed by the "full model" during a phototactic turn is shown in Fig. S8, neglecting bottom-heaviness.

The initial conditions of the model were a horizontal light direction, an upward-pointing posterior-anterior axis, and $p = h = 0$. The input parameters for the model are the following measurable quantities:

- R, the *Volvox* radius. For the simulations we used $R = 140$ μm, the mean of the populations we investigated experimentally.
- U, the translational swimming speed, which fixes the amplitude of v_0. For the simulations we used $U = 390$ μm/s, the mean of the populations we investigated experimentally.
- ω_r, the rotation rate without a light stimulus, which fixes the amplitude of w_0. For the simulations we used $\omega_r = 2.3$ rad/s, as shown in Fig. 7 of the main text.
- The θ dependence of the surface velocity. For the simulations we approximated $v_0(\theta)$ by a superposition of two associated Legendre functions, $-P_1^1(\cos\theta) + 0.25P_2^1(\cos\theta)$, as shown by the dashed magenta line in Fig. 5 of the main text. Using a simple $\sin\theta$ dependence for $v_0(\theta)$ gives qualitatively similar results. We assume that w_0 has the same θ dependence as v_0.
- $\beta(\theta)$, the responsivity of the fluid flow to light stimulation. For the full model, we used a close approximation to the $\beta(\theta)$ shown in the inset in Fig. 5*A* of the main text. For the reduced model, we used $\beta(\theta) = 0.3$, the mean of the $\beta(\theta)$ used for the full model.
- τ_r and τ_a, the response and adaptation time scales, respectively. For the simulations, we used the values measured for a light intensity of 16 μmol PAR photons $\mathrm{m}^{-2}\,\mathrm{s}^{-1}$, as displayed in Fig. 2*B* of the main text.
- τ_{bh}, the bottom-heaviness time scale, is defined by considering a flagellaless *Volvox* that is tilted at an angle ζ from the vertical. The axis of this *Volvox* would relax back to the vertical at a rate $\dot{\zeta} = -\sin(\zeta)/\tau_{\mathrm{bh}}$. For the simulations, we used $\tau_{\mathrm{bh}} = 14$ s, as measured in ref. 19.

In order to compare the results from this mathematical model with the measurements of the phototactic ability as a function of viscosity, we implemented a viscosity dependence in the model. For this we defined $\mathbf{u} = [\mathbf{u}]_w\eta_w/\eta$ and $\tau_{\mathrm{bh}} = [\tau_{\mathrm{bh}}]_w\eta/\eta_w$, where η is the viscosity and the subscript w denotes values in water.

1. Kirk DL, Kirk MM (1983) Protein synthetic patterns during the asexual life cycle of *Volvox carteri*. *Dev Biol* 96:493–506.
2. Solari CA, Ganguly S, Kessler JO, Michod RE, Goldstein RE (2006) Multicellularity and the functional interdependence of motility and molecular transport. *Proc Natl Acad Sci USA* 103:1353–1358.
3. Sakaguchi H, Iwasa K (1979) Two photophobic responses in *Volvox carteri*. *Plant Cell Physiol* 20:909–916.
4. Schletz K (1976) Phototaxis in Volvox—Pigments involved in the perception of light direction. *Z Pflanzenphysiol* 77:189–211.
5. Halldal P (1958) Action spectra of phototaxis and related problems in Volvocales, *Ulva* gametes and Dinophyceae. *Physiol Plant* 11:118–153.
6. Mast SO (1917) The relation between spectral color and stimulation in the lower organism. *J Exp Zool* 22:471–528.
7. Sineshchekov OA, Jung K-H, Spudich JL (2002) Two rhodopsins mediate phototaxis to low- and high-intensity light in *Chlamydomonas reinhardtii*. *Proc Natl Acad Sci USA* 99:8689–8694.
8. MatPIV is an open source PIV software toolbox written for Matlab. Downloads and details are at http://www.math.uio.no/~jks/matpiv/.
9. Yoshimura K, Kamiya R (2001) The sensitivity of *Chlamydomonas* photoreceptor is optimized for the frequency of cell body rotation. *Plant Cell Physiol* 42:665–672.
10. Huth K (1970) Movement and orientation of *Volvox aureus* Ehrbg. (translated from German). *Z Pflanzenphysiol* 62:436–450.
11. Harz H, Hegemann P (1991) Rhodopsin-regulated calcium currents in *Chlamydomonas*. *Nature* 351:489–491.
12. Schaller K, Uhl R (1997) A microspectrophotometric study of the shielding properties of eyespot and cell body in *Chlamydomonas*. *Biophys J* 73:1573–1578.
13. Gerisch G (1959) Cellular differentiation in *Pleodorina californica* and the organisation of colonial Volvocales (translated from German). *Arch Protistenkunde* 104:292–358.
14. Hoops HJ (1993) Flagellar cellular and organismal polarity in *Volvox carteri*. *J Cell Sci* 104:105–117.
15. Coggin SJ, Kochert G (1986) Flagellar development and regeneration in *Volvox carteri* (Chlorophyta). *J Phycol* 22:370–381.
16. Huskey RJ (1979) Mutants affecting vegetative cell orientation in *Volvox carteri*. *Dev Biol* 72:236–243.
17. Herraez-Dominguez JV, Gil Garcia de Leon F, Diez-Sales O, Herraez-Dominguez M (2005) Rheological characterization of two viscosity grades of methylcellulose: An approach to the modeling of the thixotropic behaviour. *Colloid Polym Sci* 284:86–91.
18. Stone HA, Samuel ADT (1996) Propulsion of microorganisms by surface distortions. *Phys Rev Lett* 77:4102–4104.
19. Drescher K, et al. (2009) Dancing *Volvox*: Hydrodynamic bound states of swimming algae. *Phys Rev Lett* 102:168101.
20. Solari CA, Kessler JO, Michod RE (2006) A hydrodynamics approach to the evolution of multicellularity: Flagellar motility and germ-soma differentiation in Volvocalean green algae. *Am Nat* 167:537–554.

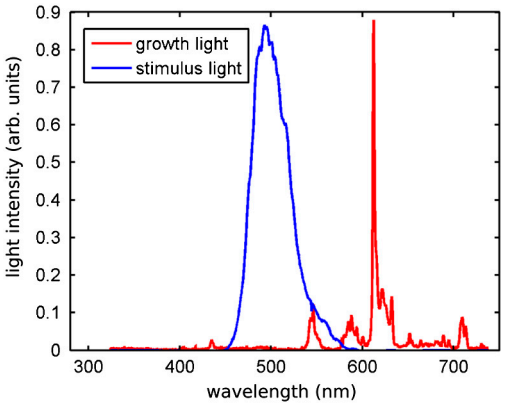

Fig. S1. Spectra of growth and stimulus light sources.

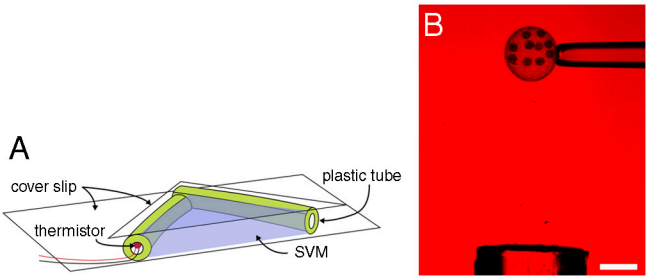

Fig. S2. (*A*) Schematic diagram of the sample chamber. (*B*) Photograph of a micropipette holding a *V. carteri* colony and the optical fiber. The colony axis is in the focal plane and pointing toward the fiber. (Scale bar: 200 μm.)

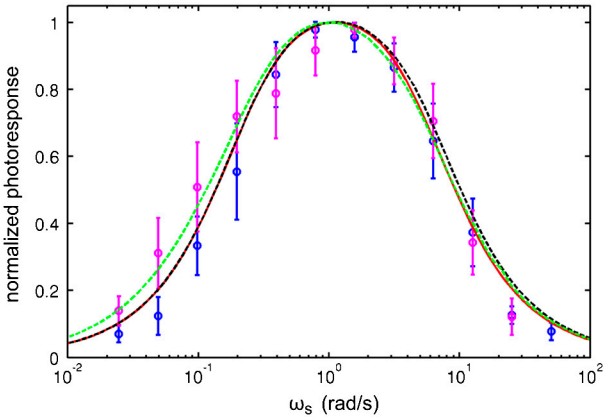

Fig. S3. Photoresponse of *V. carteri* as a function of stimulus frequency. Measurements with a sinusoidal stimulus are displayed as blue circles, measurements with a half-sine stimulus are displayed as magenta circles. The red line is a plot of Eq. **5** in the main text and therefore neglects the Heaviside function in the simple model (Eqs. **1** and **2** in the main text). The black dashed line indicates a numerical evaluation of the simple model for a sinusoidal stimulus, including the Heaviside function. The green dashed line indicates a numerical evaluation of the simple model for a half-sine stimulus, also including the Heaviside function.

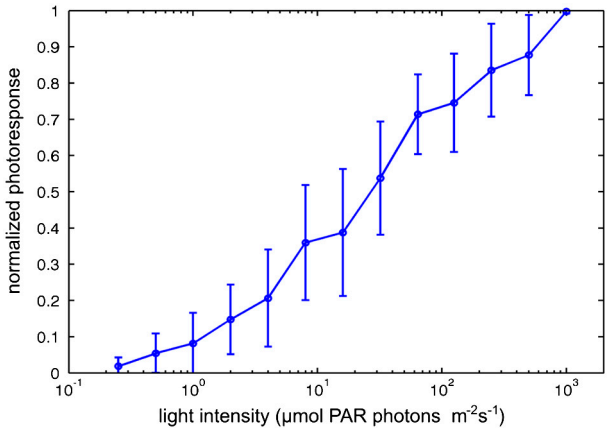

Fig. S4. The amplitude of the photoresponse for top-hat stimuli of frequency 0.25 Hz, at different stimulus light intensities.

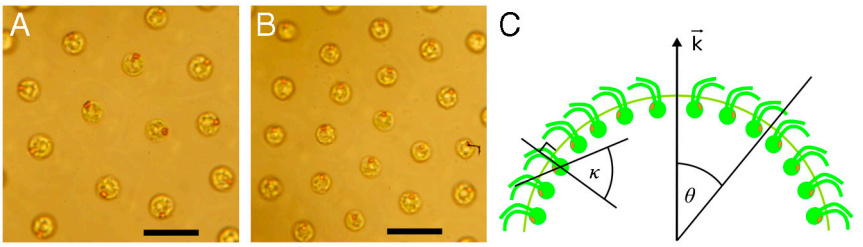

Fig. S5. (*A*) The *V. carteri* somatic cells at the anterior pole have their orange eyespots facing away from the fluid-mechanical anterior pole. (*B*) The somatic cells and eyespots at polar angle $\theta = 50°$ from the anterior. (Scale bars: 20 μm.) (*C*) Illustration of the eyespot placement in the somatic cells and the relation to the posterior-anterior axis **k**. In contrast to this schematic drawing, *V. carteri* colonies consist of thousands of somatic cells, as shown in Fig. 1*A* of the main text and as measured in ref. 20.

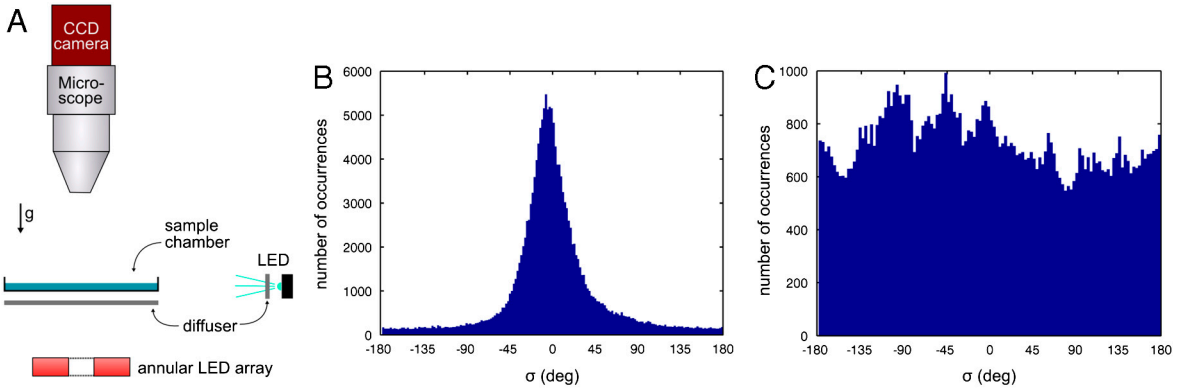

Fig. S6. (*A*) Schematic diagram of the apparatus used for the population assay. *B* and *C* show distributions of the swimming angle with the light direction σ as measured for a population at the viscosity of water (*B*) and at 40 times the viscosity of water (*C*).

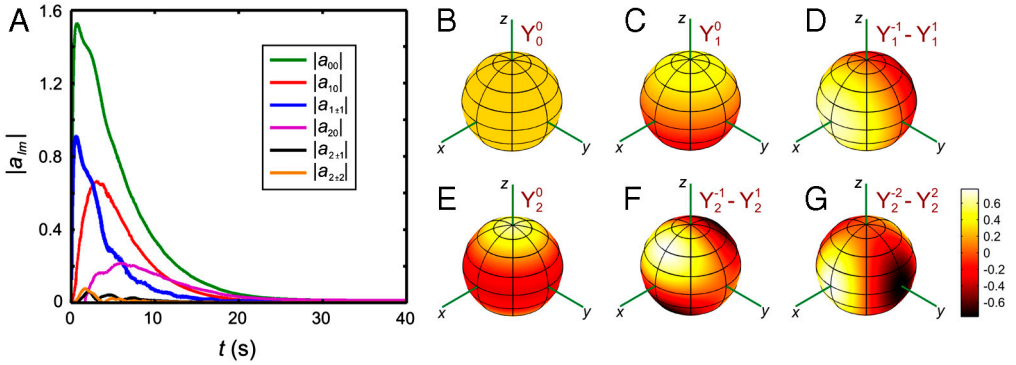

Fig. S7. The photoresponse p may be decomposed into the spherical harmonics $Y_l^m(\theta,\phi)$ via the equation $p(\theta,\phi,t) = \sum_{l,m} a_{lm}(t) Y_l^m(\theta,\phi)$. The decomposition was done for the photoresponse shown in Fig. 6 of the main text–i.e., using the reduced model. For this model, the dominant modes are the constant Y_0^0, the $Y_1^{\pm 1}$ modes that give a ϕ dependence similar to the light-shadow asymmetry, and Y_1^0, which gives an anterior-posterior asymmetry that becomes important in this model when the organism has turned significantly toward the light. *B–G* display the spherical harmonics on a sphere.

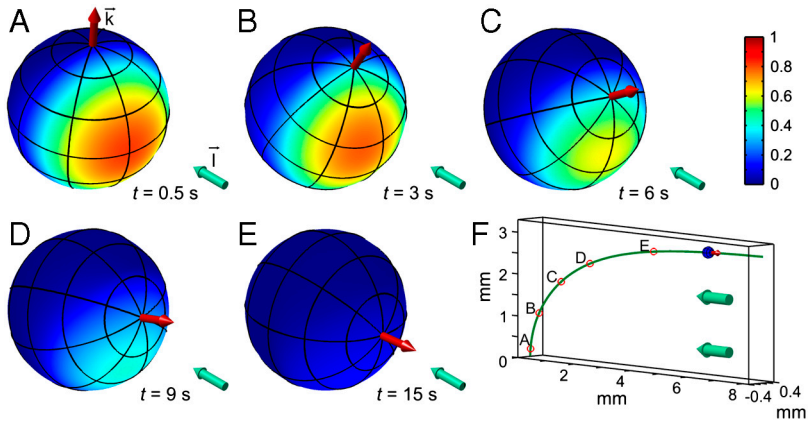

Fig. S8. The behavior of the photoresponse $p(\theta,\phi,t)$ during a phototactic turn, using the full model defined in the main text, neglecting bottom-heaviness. *A–E* show the colony axis (*Red Arrow*) tipping toward the direction of light (*Aqua Arrow*) over time. The color scheme illustrates the magnitude of p. *F* shows the location of colonies in *A–E* along the swimming trajectory.